PROCEEDINGS OF THE ROYAL SOCIETY A MATHEMATICAL, PHYSICAL & ENGINEERING SCIENCES

The Absolute Photoionization Cross Sections of Helium, Neon, Argon and Krypton in the Extreme Vacuum Ultraviolet Region of the Spectrum

J. B. West and G. V. Marr

Proc. R. Soc. Lond. A 1976 **349**, 397-421
doi: 10.1098/rspa.1976.0081

Proc. R. Soc. Lond. A. **349**, 397–421 (1976)
Printed in Great Britain

The absolute photoionization cross sections of helium, neon, argon and krypton in the extreme vacuum ultraviolet region of the spectrum

By J. B. West† and G. V. Marr‡

† *Science Research Council, Daresbury Laboratory*
‡ *J. J. Thomson Physical Laboratory, University of Reading*

(*Communicated by G. W. Series, F.R.S. – Received 8 December* 1975)

An experiment has been set up at the Daresbury Synchrotron Radiation Facility to make absolute absorption cross section measurements over a wide range of photon energies. New data are reported for helium, neon, argon and krypton over the range 340–40 Å which are believed to be reliable to ± 5 %. A critical evaluation of published cross section data has been carried out to produce best value data from the ionization thresholds throughout the vacuum ultraviolet and X-ray region. Agreement with theoretical calculations on helium is demonstrated to be within ± 2–3 % from threshold down to the double ionization threshold at 79 eV. Comparison with recent calculations of photoionization cross sections has shown that the effect of electron correlations is significant for the heavier inert gases. Contrary to previous claims, the position of the *M* shell maximum in krypton is located at 184 ± 10 eV in good agreement with r.p.a.e. calculations.

Oscillator strength sum rules have been examined and their moments calculated. Discrepancies developing towards the heavier inert gases suggests a decrease in polarizabilities and other atomic factors from those predicted by Hartree–Fock calculations.

1. Introduction

The continuous absorption of electromagnetic radiation by atoms and molecules is characterized by their photoionization cross sections evaluated as a function of the photon energy, provided the wavelengths of the radiation concerned are much larger than the atomic structure responsible for the absorption. In this, the low and intermediate energy region, the photon momentum and attendant Compton scattering effects are negligible and the hydrogenic model of the photoionization process breaks down. The average field experienced by the photoelectron departs markedly from the Coulomb law. Exchange effects and two electron transitions can be significant and the photoionization process is complicated by autoionization phenomena.

The absolute photoionization cross sections form part of the basic data for energy balance and radiation transfer processes in the fields of aeronomy, astrophysics and plasma physics. Considerable theoretical effort has now been invested in the

calculation of cross sections and oscillator strength distributions throughout the ultraviolet and X-u.v. spectral regions and various different approaches have been used to obtain the wavefunctions required in the transition matrix elements. There has been therefore a corresponding need for experimental data with which to compare theory in order to justify calculations on those atoms or ions which are difficult to study quantitatively in the laboratory. Reliable absolute atomic cross sections obtained from carefully controlled experimental conditions are required and the purpose of the present paper is to provide such data for those rare gas atoms whose resonance lines, autoionization features and continuous photoionization absorption are effectively covered by the vacuum ultraviolet region now made available through the exploitation of the electromagnetic radiation from electron synchrotrons. The use of photon counting techniques associated with the attenuation of ionizing radiation through gas cells of well defined low density has enabled a significant increase in reliability over previous measurements to be achieved. The new data are discussed in relation to previously published data, best value cross section curves are selected and oscillator strength distributions examined to look for departures from the predictions of single electron wavefunction models.

The early work on the oscillator strengths in atomic spectra, reviewed by Foster (1964), provides an adequate reference for the detailed experimental techniques. Discrete transitions have been studied, in absorption by the 'Hook' techniques (Rozhdestvenskii 1912) as later developed by Ostrovskii & Penkin (1957), in emission by zero field level crossing (Anderson 1965) by lifetime measurements (Lawrence 1968; Corney 1970) and by delayed coincidence techniques (Lewis 1967). Natural widths of the upper states of u.v. resonance lines have been measured (Kuhn & Vaughan 1964) by studying cascade processes involving visible radiation. Experimental work on autoionization features have, in general been limited to absorption techniques. Marr (1954) first obtained absolute oscillator strength data by cross section integration over the autoionization features and this has been applied to the inert gases (Pery-Thorne & Garton 1960; Huffman, Tanaka & Larrabee 1963*a*, *b* and others).

Photoionization continuum cross section measurements initially employed photographic recording techniques (Baker, Bedo & Tomboulian 1961; Lowry, Tomboulian & Ederer 1965; Marr 1967; Ederer & Tomboulian 1964) and also used Geiger counter detectors at the high energy end of the spectrum. Samson (1966) significantly improved the accuracy of the inert gas absolute cross section data by using a double ion chamber (Samson 1967). More recently synchrotron radiation has been used to provide an effective continuum for absorption measurements. Haensel, Keitel, Schreiber & Kunz (1969) reported data on krypton and xenon using the Hamburg synchrotron to make measurements in the 100–130 Å region. Watson (1972) reported cross section data on helium, neon and argon and Lang & Watson (1975) similar data for krypton and xenon in the 50–200 Å region with the Glasgow synchrotron. The National Bureau of Standards synchrotron has also been employed (Codling 1973 and references therein) to study spectral regions of inert gases where autoioniz-

ation features are apparent while Carlson, Judge, Ogawa & Lee (1973) used the Wisconsin storage ring to obtain cross section data for argon between threshold and 170 Å. The new experimental data reported in the present paper were obtained by use of the Daresbury synchrotron and covered the range 40–350 Å.

2. Experimental procedures

Until recently much of the experimental work has been carried out on total photoionization cross sections using discrete line sources or limited wavelength continua. For wavelengths less than 600 Å there are relatively few such sources.

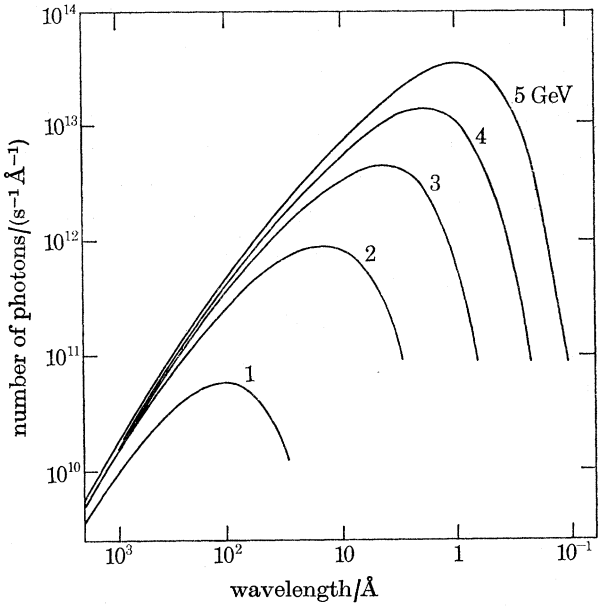

Figure 1. The abolute intensity spectrum falling onto an aperture 2 mm high × 20 mm wide, 30 m from the NINA tangent point. The curves are for different values of electron energy, and a circulating current of 20 mA.

Flash tubes have been used (see for example Balloffet, Romand & Vodar 1961; Wheaton 1964) but these are generally not consistent with a clean, high vacuum system. Because of the violent nature of such sources they are difficult to maintain, lack intensity reproducibility over long periods of time and so measurements have been in general restricted to photographic detection with the attendant intensity calibration problems. Synchrotron radiation facilities are now more generally available and such sources of ultraviolet photons overcome these difficulties. However they do introduce order sorting problems when used with conventional diffraction grating monochromators. In the present experiments these have been overcome with the use of a monochromator specifically designed to eliminate unwanted spectral orders (West, Codling & Marr 1974).

(*a*) *The synchrotron radiation source*

The electron synchrotron comes close to being the ideal source of photons in the 1–500 Å region. Its main energy-loss mechanism takes the form of electromagnetic radiation emitted as a continuum which peaks in the extreme v.u.v. and which is closely confined to the electron orbit plane. Details of the spectral characteristics of synchrotron radiation sources have been described at length elsewhere (see, for example, Codling 1973). A brief indication of those characteristics pertinent to the present measurements is included here in connection with the Daresbury electron synchrotron NINA. Typical operating electron energies are between 3 and 5 GeV with a mean circulating current of from 1 to 20 mA. The acceleration cycle is repeated 53 times a second and a typical duty cycle is 0.24. This means that the radiation is available to photoionization experiments for approximately 4.6 ms every 18.9 ms. The duty cycle is a function of photon energy and at very short wavelengths, the duty cycle is considerably reduced from that quoted because radiation in the spectral region 1–10 Å is not emitted until the electrons have been accelerated to their peak energy. Figure 1 shows the photon flux output from NINA as a function of both peak electron energy and emitted wavelength. The divergence of the beam from the orbit plane is *ca.* 0.1 mrad. at 1.5 Å and increases to *ca.* 1 mrad at 100 Å. The fluxes shown in figure 1 are integrated over the acceleration cycle and all angles above and below the orbit plane. In the region of interest for the present experiments (350–40 Å) a large proportion of the emitted radiation is collected by the monochromator.

(*b*) *The monochromator*

By careful choice of the angle of incidence and by restricting the diffraction to negative orders as described by Miyake, Kato & Yamashita (1969) the monochromator employed for the present experiments suppresses second and higher orders in the wavelength range 40–350 Å. Radiation from a slit placed close to the electron orbit is intercepted by a gold coated master grating placed 35 m from the orbit. The dispersed beam from the first negative order is then focused on to a horizontal slit by means of a suitably placed concave mirror. Grazing angles are used throughout and by proper choice of mirror focus and angle only first order radiation is transmitted with the very low stray light level ($< 1\%$ of the total output) required for absolute cross section measurements. Details of the design and performance of this instrument have been the subject of a previous publication (West *et al.* 1974).

(*c*) *The absorption cell and detection system*

Photoelectric counting techniques were used to measure simultaneously the monochromatic radiation incident upon and transmitted through the absorption gas cell shown diagrammatically in figure 2. The cell was made from stainless steel tubing, 5 cm in diameter with an effective absorption path of 160 cm. One end was terminated by a glass window and sodium salicylate screen and the other by a zapon

film *ca.* 1000 Å thick supported on an electroformed nickel mesh. Because of the spectrometer vacuum requirements 130 μPa (10^{-6} Torr), two-stage differential pumping was required between the zapon film and the monochromator. The first stage immediately followed the zapon film and was pumped by a liquid nitrogen trapped diffusion pump while the second stage comprised long differential slits leading to the monochromator. By this means pressures varying from 3 to 130 Pa (0.025 to 1 Torr) were maintained in the absorption cell while the spectrometer pressure was 260 μPa (2×10^{-6} Torr).

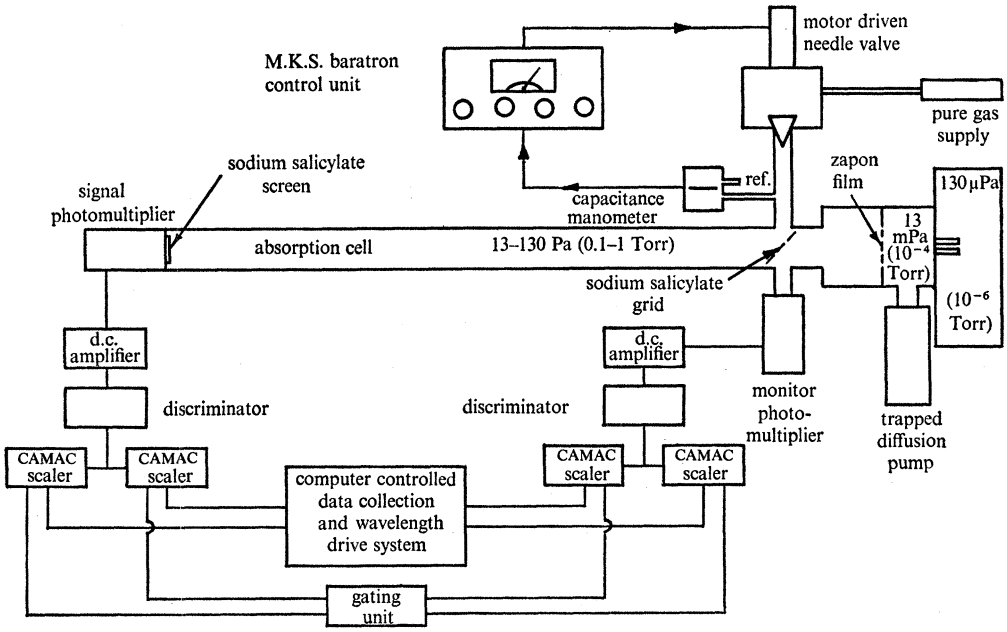

FIGURE 2. Schematic layout of absorption cell and associated control system.

The absorbing gas pressure was measured by an M.K.S. Baratron capacitance manometer whose factory calibration had been previously checked on its higher ranges by an inclined plane oil manometer. The pressure was regulated by a servo-operated needle valve driven by an error signal from the Baratron control unit. Cell pressures were maintained constant to within 65 mPa (5×10^{-4} Torr) during an experiment. Pressure gradients along the cell were reduced to negligible proportions by maintaining a cross sectional area of about 20 cm^2 throughout the cell. The wire grid monitor detector (figure 2) which defined the beginning of the absorbing column was 12 cm from the zapon window. The gas leakage through the zapon was determined to be *ca.* 650 mPa l s^{-1} so that any pressure gradient near the window was judged to extend over a region not more than 1 cm from it. Significant pressure gradients over the 160 cm absorption column were therefore eliminated, and a steady flow of gas through the cell was maintained at a selected constant pressure throughout a wavelength versus absorption cross section scan of the spectrum.

Ultrahigh purity gases from Air Products Co. were used for all measurements. The main impurities were stated to be N_2 and H_2 (*ca.* 2 p.p.m.) CO (*ca.* 1 p.p.m.), CO_2, O_2, CH_4 (*ca.* 0.5 p.p.m.) with a total impurity content of *ca.* 7 p.p.m. These impurities were not considered to introduce any significant errors into the cross sectional measurements. To overcome a possible contamination due to cell wall outgassing, careful processing of the cell was carried out prior to use. The cell was heated to 80 °C and then evacuated at 650 μPa (5×10^{-6} Torr) for 12 h. When cool the ratio of monitor to signal intensity was measured over a period of 2 h with the cell isolated from the pumping system. Only if the ratio remained constant to 0.5 % was the cell filled with the inert gas being studied. Measurements at each pressure lasted on average, 30 min, after which time the cell was evacuated before refilling with fresh gas to a new pressure. As a result of these precautions it is estimated that contamination of the gas by impurities would have added less than 0.5 % to the overall uncertainty in the final result.

The u.v. photons were detected by the sodium salicylate/photomultiplier combination employing low noise E.M.I. 9502 S photomultiplier tubes. Counts were fed into d.c. amplifiers (EG and G AN106) and thence to fast trigger units (EG and G T200N). The monochromator wavelength stepping device system and the scalers used for the photon counting were controlled on a small local computer. The CAMAC scalers shown in figure 2 were gated so that one in each channel was switched on for 4 ms during the synchrotron acceleration cycle, and the other in each channel switched on for 1 ms during the 'dark' period between electron bunches. This method enabled a continuous measurement to be made of photomultiplier dark current. The counting time for each wavelength in a run at a fixed gas pressure was always arranged to provide a statistical accuracy of 1 %. Ten different runs were made each at a different gas pressure with a spectrometer band pass of 2 Å. Wavelength calibration as verified by previous experiments, was correct to 0.25 Å and the data analysed by a least squares fit to

$$\ln (I/I_0) = -\alpha p + \text{const}, \tag{1}$$

where I_0 and I represent the incident and transmitted photon fluxes for an absorbing gas at a low pressure p (Pa), α is related to the absorption cross section σ (cm²) by

$$\alpha = \frac{\sigma T_0 l N}{P_0 T}. \tag{2}$$

T_0 and P_0 are the standard temperature and pressure, N is Loschmidt's number (cm^{-3}), l the length of the absorbing column (cm) at a temperature T (K). For convenience results are presented in Mb (1 Mb = 10^{-18} cm²) and it may be noted that the absorption cross section σ (cm²) is related to the absorption coefficient μ (cm^{-1}) by

$$\mu = N\sigma. \tag{3}$$

The constant in equation (1) represents that part of the radiation not absorbed by the gas and so was attributed to stray light in the monochromator output (< 1 % of the total absorption in all cases). With stray or scattered light levels as

low as this, the fraction of stray light contributing to the absorption coefficient μ is negligible when the least squares fit is used. The r.m.s. deviation in μ was found to be *ca.* 1 % and represents the random variation on the data. To this was added a systematic error of 2.5 % to account for uncertainties in the Baratron calibration of pressure, impurity absorptions, cell length and other small contributions. The data presented here are thus expected to have a most probable error of ± 3.5 % and a maximum error of ± 5 %.

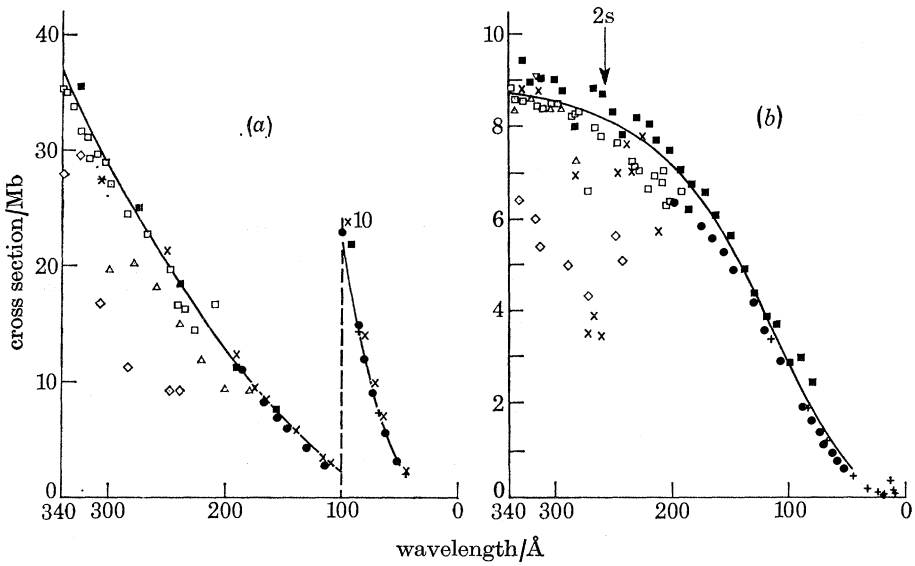

FIGURE 3. (*a*) The experimental total photoionization cross section of helium: ——, present data. (*b*) The experimental total photoionization cross section of neon: ——, present data. (The arrow indicates the 2s electron ionization threshold. For details of other authors' data see tables 2 and 3.)

(*d*) *The data analysis*

In the present experiments, an attempt has been made to examine the data for both random and systematic errors and to reduce them to a minimum consistant with the techniques available. For comparison with other published data, the following features apply:

(i) The intensity ratios of transmitted and incident fluxes were obtained from simultaneously measured values of I_0 and I corrected for dark current and averaged over a wide range of pressure for each wavelength step throughout the spectrum. Each individual intensity ratio was obtained within a stipulated accuracy of 1 %.

(ii) The length of the absorption cell was precisely determined in the absence of end effects to an accuracy of 0.25 %.

(iii) The cell was constructed to minimize pressure gradients along its length and was long enough to ensure that equation (1), the Lambert–Beer Law applies.

(iv) The monochromator was designed to remove higher order radiation. The

low intensity scattered light, most of which was accounted for automatically by the data processing has $\ll 1\ \%$ effect on the final results.

(v) The absorption cell is located after the monochromator exit slit so minimizing population variations due to photon excitation.

(vi) Contamination from impurity species was minimized by careful outgassing and the use of slow gas flow techniques. The effect of extraneous absorption is $< 0.5\ \%$ of the final results.

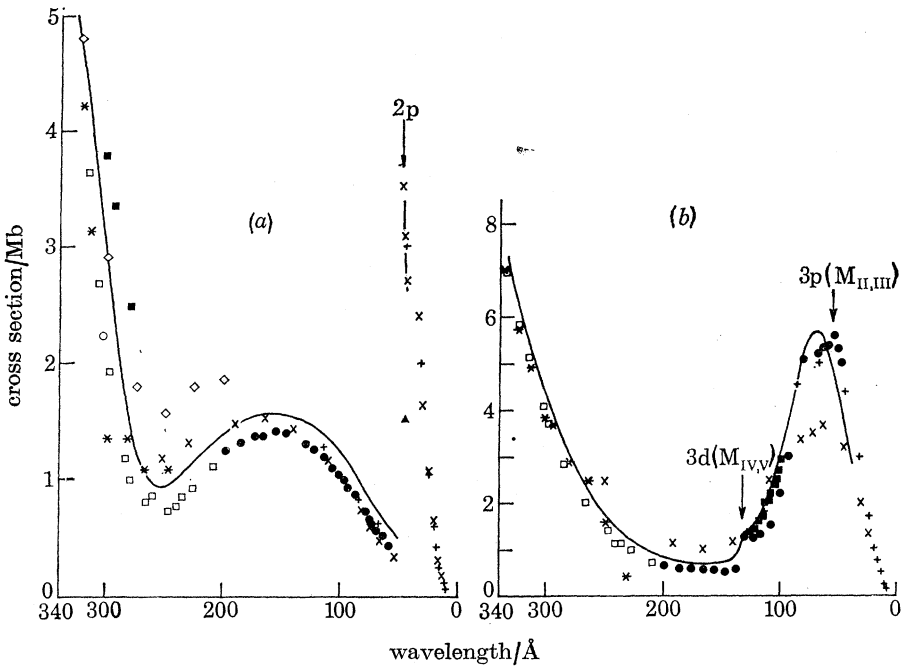

FIGURE 4. (*a*) The experimental total photoionization cross section of argon. (The arrow indicates the mean values of the 2p electron ionization thresholds.) ——, Present data. (*b*) The experimental total photoionization cross section of krypton. (The arrows indicate the mean values of the 3d and 3p ionization thresholds.) ——, Present data. For details of other authors' data see tables 4 and 5.

(vii) The gas pressure was kept constant throughout each experiment by an automatic needle valve system.

(viii) A stable, clean and reproducible source of continuous radiation was available from the NINA synchrotron throughout the entire wavelength range of measurement.

It is believed that the cross sections presented here in figures 3 and 4 are among the most reliable obtained to date for helium and neon and for argon and krypton respectively. Data from previous publications is shown for comparison and it is clear that although there are no large discrepancies, the present measurements help to remove uncertainties in previous data. In carrying out the measurements for the

TABLE 1. THE TOTAL PHOTOIONIZATION CROSS SECTIONS OF HELIUM, NEON, ARGON AND KRYPTON

	cross-section/Mb			
wavelength/Å	He	Ne	Ar	Kr
884	—	—	—	29.6
880	—	—	—	30.8
860	—	—	—	35.8
840	—	—	—	39.1
820	—	—	—	41.2
800	—	—	—	42.3
783	—	—	29.2	—
780	—	—	29.5	42.8
760	—	—	31.1	42.9
740	—	—	32.5	42.7
720	—	—	33.7	42.2
700	—	—	34.7	41.7
680	—	—	35.5	41.0
660	—	—	36.1	40.2
640	—	—	36.5	39.3
620	—	—	36.7	38.3
600	—	—	36.7	37.1
580	—	—	36.5	35.7
575	—	6.21	—	—
570	—	6.33	—	—
560	—	6.58	36.1	34.2
540	—	7.05	35.4	32.4
520	—	7.47	34.4	30.4
504	7.56	—	—	—
500	7.46	7.83	33.1	28.2
480	6.94	8.15	31.4	25.8
460	6.43	8.42	29.5	23.2
440	5.93	8.64	27.1	20.6
420	5.45	8.80	24.3	17.8
400	4.98	8.91	21.0	15.1
380	4.53	8.96	17.1	12.5
360	4.09	8.95	12.8	9.96
340	3.68	8.89	7.77	7.67
320	3.27	8.77	4.62	5.66
300	2.89	8.58	2.47	3.98
290	2.70	8.47	1.77	3.43
280	2.52	8.34	1.30	2.93
270	2.35	8.19	1.03	2.47
260	2.18	8.03	0.914	2.05
250	2.02	7.85	0.916	1.68
240	1.86	7.66	1.00	1.36
230	1.70	7.45	1.13	1.11
220	1.55	7.23	1.28	0.943
210	1.41	6.98	1.36	0.838
200	1.28	6.72	1.42	0.789
190	1.14	6.45	1.45	0.737
180	1.02	6.15	1.48	0.697
170	0.903	5.84	1.48	0.671
160	0.792	5.52	1.47	0.652
150	0.687	5.17	1.45	0.633
140	0.588	4.81	1.41	0.607
130	0.497	4.43	1.36	1.18
120	0.412	4.03	1.29	1.55
110	0.335	3.50	1.20	2.04
100	0.265	2.98	1.10	2.97

PROCEEDINGS OF THE ROYAL SOCIETY A MATHEMATICAL, PHYSICAL & ENGINEERING SCIENCES

TABLE 1 (*cont.*)

wavelength/Å	cross section/Mb			
	He	Ne	Ar	Kr
95	0.233	2.71	1.05	3.50
90	0.202	2.44	0.987	4.01
85	0.174	2.18	0.923	4.49
80	0.147	1.92	0.856	4.88
75	0.123	1.66	0.785	5.16
70	0.100	1.43	0.709	5.31
65	0.0795	1.22	0.630	5.31
60	0.0609	0.992	0.547	5.16
55	0.0443	0.792	0.461	4.88
50.5	—	—	4.77	—
50	0.0315	0.620	4.66	4.47
45	0.0235	0.472	3.64	3.97
40	0.0168	0.348	2.76	3.41
35	0.0114	0.247	2.02	2.82
30	0.00736	0.166	1.41	2.24
25	0.00437	0.104	0.920	1.68
22.5	0.00323	—	—	—
20	0.00231	0.0582	0.546	1.17
18	0.00171	0.0444	0.426	0.933
17.5	0.00157	—	—	—
16	0.00122	0.0328	0.324	0.708
15	0.00101	0.0277	0.278	0.610
14.3	—	0.0245	—	—
14	0.000832	0.367	0.237	0.520
13	0.000673	0.300	0.199	0.438
12.5	0.000601	—	—	—
12	0.000535	0.241	0.165	0.363
11	0.000417	0.190	0.135	0.300
10	0.000318	0.147	0.108	0.237
9	0.000235	0.110	0.0842	0.186
8	0.000168	0.0800	0.0639	0.141
7	0.000115	0.0556	0.0467	0.756
6	0.000074	0.0366	0.0326	0.502
5	0.000044	0.0223	0.0213	0.310
4	0.000023	0.0121	0.0126	0.171
3.86	—	—	0.100	—
3.8	—	0.0105	0.0959	0.150
3.6	—	0.00910	0.0826	0.130
3.4	—	0.00779	0.0706	0.111
3.2	—	0.00661	0.0599	0.0949
3.0	0.000010	0.00554	0.0501	0.0800
2.8	—	0.00459	0.0414	0.0666
2.6	—	0.00376	0.0338	0.0548
2.4	—	0.00302	0.0271	0.0443
2.2	—	0.00238	0.0213	0.0352
2.0	0.000003	0.00184	0.0164	0.0273
1.8	—	0.00138	0.0123	0.0207
1.6	—	0.00100	0.00889	0.0151
1.5	0.000001	—	—	
1.4	—	0.000697	0.00616	
1.2	—	0.000458	0.00403	
1.0	—	0.000279	0.00244	
0.8	—	0.000152	0.00132	
0.6	—	0.000069	0.000599	
0.4	—	0.000023	0.000196	
0.2	—	0.000003	0.000029	

present data, wavelengths where structure is known to be present (e.g. in neon, the lines of autoionizing series $1s^2\,2s^2\,2p^6\,(^1S_0) \rightarrow 1s^2\,2s\,2p^6\,np(^1P_1)$ between 250 and 300 Å) were avoided. The data therefore strictly reflects the continuous photoionization absorption cross sections only and the error bars shown are for the maximum possible error ($\pm 5\,\%$) as discussed above.

(*e*) *The critical evaluation of cross section data*

While it is believed that the present data are well established and reliable, it is possible to reduce still further the systematic errors by combining the data with

TABLE 2. HELIUM

wavelength range/Å	origin of experimental data	symbol used on figure 3*a*
93–504	Baker *et al.* (1961)	■
	Lowry *et al.* (1965)	■
304–498	Cairns & Samson (1965)	*
239–492	Lee & Weissler (1955)	◇
46–338	Present data	—
44.6–113.8	Henke *et al.* (1967)	+
44.6	Dershem & Schein (1931)	▲
44.4–250.5	Lukirskii *et al.* (1964)	×
179–299	Axelrod & Givens (1959)	△
53.1–186	Watson (1972)	●
209.3–503	Samson (1966)	□
1.54–4.15	Bearden (1966)	not plotted
1.0–17.67	Compton & Allison (1967)	not plotted

those of other workers and to obtain a best value curve by fitting a polynomial to the weighted data points. The weighting of the data is in general a difficult matter to decide and the following criteria were adopted.

(i) Number and consistency (i.e. the freedom from scatter of data points).

(ii) Amount of information given on the experimental technique.

(iii) Characteristics of the source used.

(iv) Performance and quality of the monochromator used.

(v) The proportion of the features (i)–(viii) from §(*d*) involved in the data determination.

In the region between 40 and 350 Å the present new data were given a weight of unity. In those regions outside the wavelength range of the present measurements, the best measurements from other workers according to the criteria (i)–(v) above were also given a weight of unity. The polynomial curve fitting procedure was used over sections of the continuum between edge discontinuities so that features such as the 2p threshold in argon at 50.6 Å were not smeared out. Regions containing autoionization structure were assumed to be continuous and were accounted for separately when oscillator strength sum rules were applied.

The uncertainties in the final values of the cross sections derived from weighted

means were calculated from the r.m.s. deviations in the polynomial coefficients and in general a probable error of between 2 and 3 % resulted. This varied according to the scatter in published data and was most serious in the region between 350 Å and the onset of photoionization for all of the gases. Where there was good agreement between present data and published data within the wavelength range of the present measurements, it was assumed that the data of other authors was equally reliable

TABLE 3. NEON

wavelength range/Å	origin of experimental data	symbol used on figure 3*b*
243–575	Lee & Weissler (1953)	◇
83.5–558.5	Ederer & Tomboulian (1964)	■
190–575	Samson (1965)	□
192.9–573.5	Samson (1966)	□
53.2–199	Watson (1972)	●
211–575	Ditchburn (1960)	×
45.4–338	Present data	—
282–574	Comes & Elzer (1964)	△
1–8	Wuilleumier (1963)	not plotted
8.34–113.8	Henke *et al.* (1967)	+
1.54–14.6	Bearden (1966)	not plotted

TABLE 4. ARGON

wavelength range/Å	origin of experimental data	symbol used on figure 4(*a*)
600–770	Huffmann *et al.* (1963*a*)	not plotted
246–778	Rustgi (1964)	*
600–780	Metzger & Cook (1965)	not plotted
304–780	Cairns & Samson (1965)	○
450–781	Blackwell *et al.* (1964)	not plotted
200–700	Carlson *et al.* (1973)	◇
475–769	Wainfan *et al.* (1955)	not plotted
45.5–329	Present data	—
281–574	Comes & Elzer (1964)	not plotted
209.3–783.2	Samson (1966)	□
57.1–199	Watson (1972)	●
8.34–113.8	Henke *et al.* (1967)	+
44.6	Dershem & Schein (1931)	▲
4–251.5	Lukirskii & Zimkina (1963)	×
0.59–8	Wuilleumier (1963)	not plotted
1.54–14.6	Bearden (1966)	not plotted

outside the range of the present measurements. Thus in the long wavelength region, the data of Samson (1966) and in the short wavelength region the data of Henke, Elgin, Lent & Ledingham (1967) were given unit weight. An abbreviated tabulation of the best value data from the analysis is collected together in table 1 for helium. neon, argon and krypton respectively. In tables 2–5 a list of authors whose data has been used is presented together with information on the spectral range of their measurements. Extensive tabulation of the critically evaluated data appears in Marr & West (1976).

Analysis of the discrete autoionization data has been carried out by several workers (see Samson 1966; Codling 1973). In this paper we are concerned with oscillator strength distributions over extended photon energy ranges. We have therefore taken smoothed values through published cross section data in order to examine f-sum contributions. In all cases the errors introduced in the estimation of the f-sums due to autoionization features is $\ll 1\,\%$.

TABLE 5. KRYPTON

wavelength range/Å	origin of experimental data	symbol used on figure 4*b*
501–852	Blackwell *et al.* (1964)	not plotted
600–840	Metzger & Cook (1965)	not plotted
504–842	Pery-Thorne & Garton (1960)	not plotted
230–786	Rustgi *et al.* (1964)	*
99–131	Haensel *et al.* (1969)	■
209.3–883.6	Samson (1966)	□
39.5–343	Present data	—
48.9–198	Lang & Watson (1975)	●
44.6	Dershem & Schein (1931)	not plotted
8.34–113.8	Henke *et al.* (1967)	+
23.6–250.5	Lukirskii *et al.* (1964)	×
15.0–1.5	Wuilleumier (1972)	not plotted

3. THE CALCULATION OF OSCILLATOR STRENGTHS AND CROSS SECTIONS

The oscillator strength, or f-value of a transition can be readily defined in terms of the eigenfunctions of the Schrödinger equation so that its calculation follows a well defined mathematical procedure. However, it can only be carried through for a many electron atom in an approximate form. The same is true for the absorption cross section (σ) integrated over the line shape. In the central-field one-electron approximation they are related by (Bethe & Salpeter 1957).

$$f_{n,l}^{n',l\pm1} = \frac{1}{3}\frac{l_{\max}}{2l+1}(\epsilon_{n',l\pm1}-\epsilon_{n,l})\left|M_{n,l}^{n',l\pm1}\right|^2$$
$$= \frac{mc}{\pi e^2}\int\sigma(\epsilon)\,\mathrm{d}\epsilon, \qquad (4)$$

where $M_{n,l}^{n',l\pm1}$ is the electric dipole transition moment for the bound–bound transition defined by the quatum numbers, n, l and n', $l\pm1$ and expressed in atomic units of $a_0(a_0 = 5.292\times10^{-9}\,\mathrm{cm})$. For transitions to the $l-1$ states, $l_{\max} = l$, while for the alternative $l+1$ series, $l_{\max} = l+1$. The eigenvalues, $\epsilon_{n,l}\,\epsilon_{n',l\pm1}$ for the initial and final states respectively are expressed in Rydbergs and the other symbols have their usual meanings.

The discrete absorption spectrum of an atom consists of Rydberg-like series whose frequencies and f-values are distributed in a regular manner to converge on to the ionization threshold associated with the photoionization continuum. The

features of the high series members of the discrete spectrum are determined by the circumstances affecting a particular electron which, having received energy by photo-absorption, begins to move outwards from the rest of the atom. The electron is constrained primarily by Coulomb attraction to the core as though it belonged to a hydrogenic atom. Whether the electron will escape or not depends on the total and potential energies well outside the remainder of the atom. If it remains bound the eigenvalue of the excited state may be written in the form

$$\epsilon_{n'} = -(1/n'^{*2}), \tag{5}$$

Where n'^* is the effective principal quantum number and the oscillator strength distribution for unit energy interval takes the form (Marr & Creek 1968)

$$\mathrm{d}f_{n'}/\mathrm{d}\epsilon = \tfrac{1}{2}n'^{*3}f_{n'}. \tag{6}$$

This oscillator strength concept can be extended formally into the photo-ionization continuum by

$$\frac{\mathrm{d}f^{\epsilon,l\pm1}_{n,l}}{\mathrm{d}\epsilon} = \frac{1}{3}\frac{l_{\max}}{2l+1}(\epsilon_{l\pm1}-\epsilon_{n,l})\,|M^{\epsilon,l\pm1}_{n,l}|^2$$
$$= \frac{mc}{\pi e^2}\sigma(\epsilon), \tag{7}$$

where the bound-free matrix element $M^{\epsilon,l\pm1}_{n,l}$ is normalized per unit energy of the emitted electron. It is to be expected therefore that the oscillator strength distribution $\mathrm{d}f/\mathrm{d}\epsilon$ varies smoothly from the discrete states defined by equation (6) to that of the associated continuum defined by equation (7).

The basic quantity in the oscillator strength calculation is the matrix transition element which takes the form

$$M^{n',l\pm1}_{n,l} = \int_0^\infty P_{n,l}(r)\,rP_{n',l\pm1}(r)\,\mathrm{d}r. \tag{8}$$

In the single electron approximation, $P_{n,l}$ is a solution of the radial equation

$$\frac{\mathrm{d}^2P_{n,l}}{\mathrm{d}r^2} + \frac{2m}{\hbar^2}\left[\epsilon_{n,l} - V(r) - \frac{l(l+1)\,\hbar^2}{2mr^2}\right]P_{n,l} = 0, \tag{9}$$

where $V(r)$ is a central field potential chosen to represent that experienced by the electron. Each electronic state of the atom is described by a single configuration defined by the quantum numbers n, l, m, s applicable to particles moving in a central field without any appreciable spin-orbit coupling. The wavefunction for the atom is then approximated as an antisymmetrized product of one electron functions or orbitals. In the simplest form $V(r)$ is taken to be Coulombic in which case the radial functions P and the integrals M have analytic expressions. For a discussion of the various one-electron models see Fano & Cooper (1968) and Weiss (1970). They are limited in that the electron interactions are approximated by an averaged localized potential $V(r)$.

In order to outline the development of the atomic model calculations, it is convenient to resolve a photo-absorption process into two stages. In the first, the photo-

absorption 'proper' (Fano & Cooper 1968) takes place in that region of space occupied by the initial orbital. This is then followed by the 'escape' of the electron to another region which in general is further removed from the nucleus or in fact may result in the loss of the electron from the atom altogether. This escape of the electron through the outer layers of the atom physically enables us to describe the corrections necessary to account for the experimental distribution of oscillator strength through phenomena which can modify the escape probability by reflexion or penetration of potential barriers. Details of individual processes are to be found in Fano & Cooper (1968), Amusia (1974), and Crasemann (1975).

To include electron–electron interactions, the many electron model has to be invoked. In its simplest form, the wavefunction is approximated as a linear combination of configurations which involve the antisymmetrized products of atomic one electron orbitals. However, it often happens that one configuration dominates the wavefunction so that it is not necessary to abandon the single configuration picture completely. Instead it becomes the zero order starting point with all remaining terms representing small corrections to the wavefunctions.

For atomic states of all but the lightest atoms, best-wavefunction calculations have proceeded by way of the Hartree–Fock method. Here the wavefunctions Ψ_0, $\Psi_{n,l}$ are expressed as Slater determinants of single-electron wavefunctions with the radial functions $P_{n,l}(r)$ defined by requiring

$$E_{\mathrm{s}} = \frac{\langle \Psi_{\mathrm{s}} | \mathscr{H} | \Psi_{\mathrm{s}} \rangle}{\langle \Psi_{\mathrm{s}} | \Psi_{\mathrm{s}} \rangle} \tag{10}$$

to be a minimum with respect to variation of ψ_{s}.

$\mathscr{H}$ is the Hamiltonian for an atom with atomic number Z and N electrons and has the form

$$\mathscr{H} = \sum_j \left\{ \frac{P_j^2}{2m} - \frac{Ze^2}{r_j} + \sum_{i=j+1}^{N} \frac{e^2}{|r_i - r_j|} \right\}. \tag{11}$$

This leads to an equation for $P_{n,l}(r)$ different from the one electron model in that

$$\frac{\mathrm{d}^2 P_{n,l}(r)}{\mathrm{d}r^2} + \frac{2m}{\hbar^2}\left[\epsilon_{n,l} - V_{n,l}(r) - \frac{l(l+1)\,\hbar^2}{2mr^2}\right] P_{n,l}(r) = X_{n,l}(r, P_{n,l}) + \sum_{n'\lambda n} \lambda_{nn'} P_{n'l}(r). \tag{12}$$

The central potential $V_{n,l}(r)$ now is different for different subshells and so depends on wavefunctions $P_{n'l}(r)$ for the other electrons, $X_{n,l}$ is added to represent the effect of electron exchange on $P_{n,l}(r)$ and introduces a non-local potential into the problem. Equation (12) represents in fact a system of coupled equations which now have to be solved simultaneously instead of independently as in the one electron model. The calculation of continuum radial wavefunctions in the Hartree–Fock approximation proceeds under the assumption that $P_{n'l}(r)$ becomes small in the region of r where it overlaps with the wavefunctions of the other electrons as $n' \to \infty$. The calculation can therefore proceed by two steps. In the first, the wavefunctions of the bound electrons are calculated as though the bound electrons are associated with a positive ion and, secondly, the equation (12) is solved for the continuum electron

utilizing the previously calculated wavefunction of the bound electrons to determine $X_{n,l}$ and $V_{n,l}$. This computation yields therefore an approximate value of the continuum wavefunction which may be improved by the inclusion of configuration interactions and correlations between electrons and electron subshells (see Burke & Taylor 1975; Chang & Poe 1975) by many-body perturbation theory. The exchange potential $X_{n,l}$ in the Hartree–Fock formalization introduces a non-localized potential into the calculation which give rise to differing expressions for the oscillator strength distributions depending on whether the electric dipole length or velocity formulae are used.

Another approach to the calculation of the matrix transition elements has become effective in recent years under the name of the random phase approximation. Developed originally to study an infinite many-body electron gas (Bohm & Pines 1953; Bohm 1953) it was adapted (Altick & Glassgold 1964) to the study of correlation effects in atoms. Based on a statistical model of the atomic electrons, it assumes that the outer and intermediate electron shells, where the average distance between electrons is much smaller than the effective radius of the interaction between them, behave like a high density electron gas. It has the advantage (Fano & Cooper 1968; Crasemann 1975) that it is not necessary to calculate in detail the wavefunctions for both the initial and final states but only those differences between them which are relevant to the calculation of the oscillator strength. The Hartree–Fock wavefunctions are still employed as the zero order functions so that electron exchange effects are automatically included (Amusia 1974) giving rise to the random phase approximation with exchange (r.p.a.e.) calculations. The introduction of electron correlation effects is simultaneously included in both the initial and final states in contrast to the many-body perturbation theory models in which the wavefunctions have to be individually evaluated.

(*a*) *The photoionization cross sections: a comparison between theory and experiment*

Calculations of the atomic properties of many electron atoms are limited by the approximate nature of the wavefunctions involved. In general it is difficult to estimate the magnitude of the errors which may be present and for this reason detailed comparison with experimental data is required. The photoionization cross section of atomic helium has been calculated by many authors using the Hartree–Fock approach and modifications to include electron correlation through the introduction of core polarization in the calculation of the continuum wavefunction. Very accurate ground state wavefunctions (Weiss 1967) are now available which involve up to 50 parameters and the cross sections have been tabulated (Bell & Kingston 1970) making possible a comparison between dipole length and velocity formulae which show that the dipole velocity computations converge more rapidly to a constant value than those of the dipole length model when increasingly accurate ground state functions are used. However, their analysis also shows that the velocity formulae is much more sensitive to the choice of a free state wavefunction. An

alternative approach by Bell & Kingston (1967) involved modifications to the cross section values by use of oscillator strength sums and comparison with other atomic data (see § 4). Their modified cross section values (Bell & Kingston 1970) are estimated to be accurate to about ± 1 % at the low photon energies encountered in the v.u.v.

Table 6 shows a comparison of the calculated cross section values of Bell & Kingston (1970) with the best value data of § 2. For energies below the onset of double ionization (79 eV) the modified cross section values (column 3) are generally within 2–3 % of our best value data with the exception of threshold (3.5 %) and

TABLE 6. CROSS SECTION VALUES/Mb FOR HELIUM

energy / eV	expt. best value ± 3 %	modified calc.	*L* polarized	*V* polarized	*L* Hartree–Fock	*V* Hartree–Fock	energy / Rydberg
24.60	7.56	7.307	7.573	7.846	7.330	7.156	0
25.96	6.87	6.761	6.996	7.245	6.786	6.616	0.1
27.32	6.40	6.256	6.464	6.693	6.281	6.116	0.2
31.40	4.87	4.979	5.132	5.307	4.999	4.851	0.5
38.20	3.36	3.489	3.602	3.706	3.509	3.382	1.0
51.80	1.85	1.896	1.972	1.994	1.907	1.811	2.0
65.40	1.14	1.146	1.191	1.187	1.143	1.074	3.0
74.00	0.791	0.745	0.7719	0.7579	0.7341	0.6842	4.0
133.4	0.221	0.204	0.2036	0.1932	0.1916	0.1752	8.0
242.2	0.0349	—	0.03491	0.03383	0.03477	0.3152	16.0
459.8	0.00542	—	0.004093	0.004523	0.004803	0.004416	32.0
895.0	0.000844	—	0.0004167	0.0005234	0.0005581	0.0005275	64.0
4146.8	0.0000100	—	0.00004565	0.00005639	0.00005920	0.00005738	128.0

Theoretical data from Bell & Kingston (1970).
L denotes dipole length.
V denotes dipole velocity.
Polarized and Hartree–Fock denote the form of the final wave function with 50 parameter ground state functions.

around 40 eV (3.7 %). The good agreement between the modified theory and experiment provides a reliable external check on our best value analysis which is estimated to have a maximum probable error of between 2 and 3 %. Comparison with dipole length (*L*) and velocity (*V*) calculations using 50 parameter ground state functions and H.F. or polarized orbital free state functions does not reveal any overall advantage. An average of the four sets of calculated cross sections (columns 4–7) again brings the data into very good agreement with the experimental best values except in the region of 30–50 eV, where it is 4–5 % too high. Serious discrepancies between theory and experiment now lie only beyond the threshold for double ionization which is at 79 eV.

Such detailed comparisons are not available for the other inert gases. However, it is well known that correlation effects become increasingly important for the heavier inert gases. In figures 5–7, we compare the experimental best value data

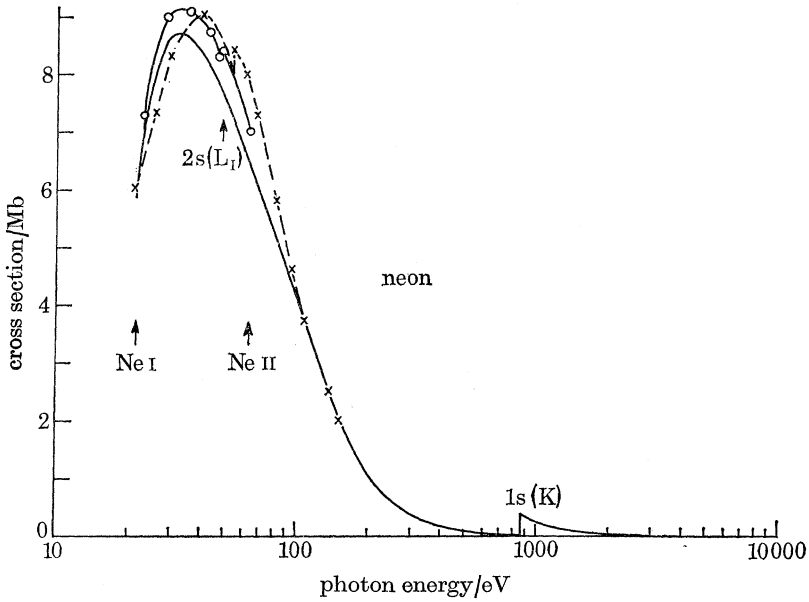

FIGURE 5. Best value data for neon compared with theoretical calculations. ×, Amusia *et al.* (1971) R.P.A.E. method. ○, Burke & Taylor (1975) R-matrix method. The thresholds for single ionization, double ionization, 2s and 1s electron ionization are shown.

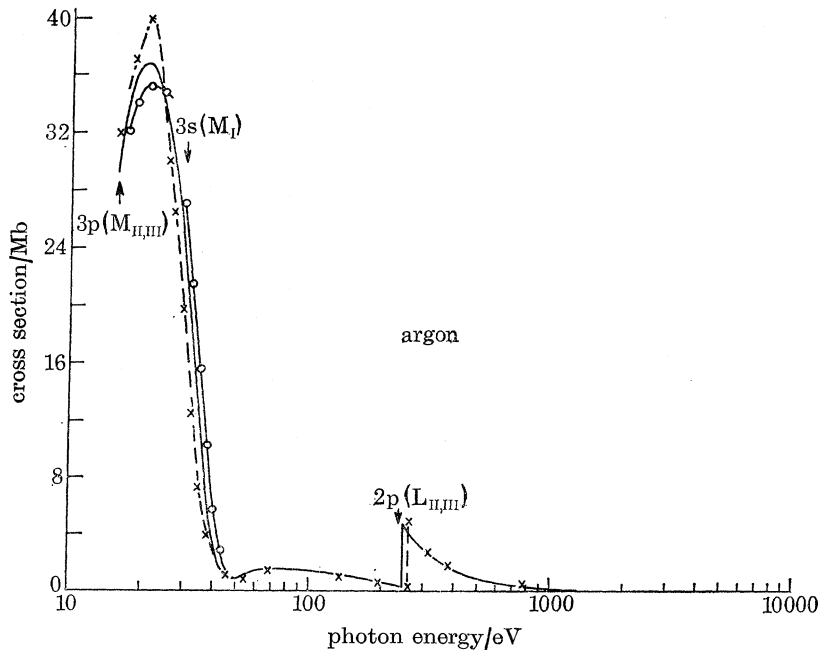

FIGURE 6. Best value data for argon compared with theoretical calculations. ×, Amusia *et al.* (1971) R.P.A.E. method. ○, Burke & Taylor (1975) R-matrix method. The thresholds for 3p, 3s and 2p electron ionization are shown.

with recent calculations of Burke & Taylor (1975) using R matrix theory and the r.p.a.e. calculations of Amusia, Cherepkov & Chernysheva (1971). Only the dipole length formulation has been used in presenting the data from Burke & Taylor. The dipole velocity curves are slightly lower. In the r.p.a.e. calculations, differences between the dipole length and velocity values are within 5 %. The inclusion of electron correlations have greatly improved the agreement between theory and experiment, however some discrepancies still remain (*ca.* 10–15 %) and more detailed comparisons require detailed tabulations of the calculated cross-section values.

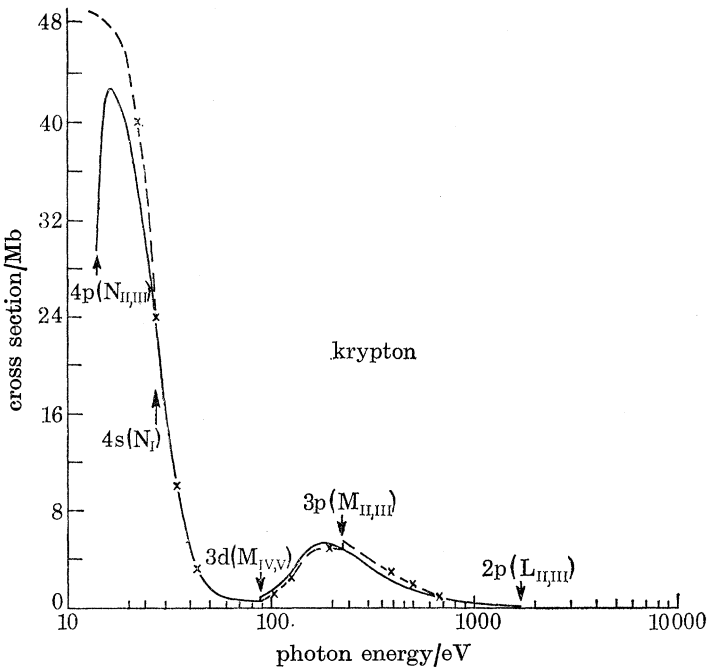

FIGURE 7. Best value data for krypton compared with theoretical calculations by Amusia *et al.* (1971) ×, r.p.a.e. method. The thresholds for 4p, 4s, 3d, 3p and 2p electron ionization are shown.

From their recent photographic studies Connerade & Mansfield (1975) claim to have located the position of the M shell maximum in krypton at 157 ± 6 eV and suggest that there is a significant deviation between theory and experiment in the determination of this maximum. Our experimental data and those of previous workers do not substantiate this claim. We find that the maximum occurs at 184 ± 10 eV in very good agreement with the calculations of Amusia *et al.* (1971). The claims of Connerade & Mansfield are based on the assumption of the linearity of their photographic emulsion and the complete absence of higher order radiation from their diffraction grating. The discrepancy between their relative data and the present absolute cross section data would suggest that extreme caution should be used in interpolation from photographic plate densities to cross sections.

Discrepancies between theory and experiment in krypton still remain in that the calculations are low by < 1 Mb while the region above the L edge is high by a similar amount.

4. The oscillator strength moments and sum rules

Within the single electron wavefunction framework, the Rydberg series plus its associated photoionization continuum may be represented by an oscillator strength sum (Bethe & Salpeter 1957) equal to the number of electrons in the subshell. A more general description of the spectral distribution is also possible through the energy moments of the oscillator strength, to give

$$S_r = \sum_{n'=1}^{\infty} \epsilon_{n'}^r f_{n'} + \int_I^{\infty} \epsilon^r \frac{\mathrm{d}f}{\mathrm{d}\epsilon} \mathrm{d}\epsilon, \tag{13}$$

where I is the ionization threshold and r is an integer. In the non-relativistic approximation, the spectral density of the oscillator strength decreases for large ϵ as

$$\mathrm{d}f/\mathrm{d}\epsilon \approx \epsilon^{-\frac{7}{2}} \tag{14}$$

so that S_r becomes infinite for $r > 2$. However, for $r \leqslant 2$ the various S_r are related to atomic properties so that (Fano & Cooper 1968).

$$S_{-2} = \tfrac{1}{4}\alpha, \tag{15}$$

$$S_{-1} = \tfrac{1}{3}\langle \Psi_0 | (\textstyle\sum_i r_i)^2 \Psi_0 \rangle, \tag{16}$$

$$S_0 = N, \tag{17}$$

$$S_{+1} = \tfrac{4}{3}\{E_0 + \tfrac{1}{2}\textstyle\sum_{i \neq j} \langle \Psi_0 | \boldsymbol{p}_i \cdot \boldsymbol{p}_j | \Psi_0 \rangle\}, \tag{18}$$

$$S_{+2} = \frac{16\pi Z}{2} \sum_i \langle \Psi_0 | \delta(r_i) | \Psi_0 \rangle, \tag{19}$$

where α is the polarizability of the atom in units of a_0^3 and S_{-1} is related to the diamagnetic susceptibility χ per mole by (van Vleck 1932)

$$\chi = -7.92 \times 10^{-7} [3S_{-1} - \sum_{i \neq j} \Psi_0 | \boldsymbol{r}_i \cdot \boldsymbol{r}_j | \Psi_0].$$

S_0 represents the Thomas–Reiche–Kuhn sum rule, S_{+1} involves the binding energy E_0 of the electrons and S_{+2} contains a measure of the electron density at the nucleus.

Previous evaluations of S_r have been carried out by Ederer & Tomboulian (1964) and by Piech & Levinger (1964) for neon, and by Baker *et al.* (1961) and Lowry *et al.* (1965) for helium. Bell & Kingston (1967) used the sum rules as a check and to improve calculated wavefunctions of helium. Table 7 presents an updated evaluation obtained from the best value data from table 1 and compares it with the Hartree–Fock calculations. Within the framework of the one electron wavefunction model, Pauli forbidden transitions to filled inner shells have to be included in the summations (Unsöld 1955). These have been calculated for individual subshells by

using Hartree–Fock wavefunction tabulations of Froese–Fischer (1972) via equation (4). The critical data compilations on atomic transition probabilities (Wiese, Smith & Glennan 1966; Wiese, Smith & Miles 1969) were used as starting points for the estimation of oscillator strength contributions from discrete transitions for helium, neon and argon. These have been augmented by data from the review of Samson (1966), calculations by Cooper (1962) and by Amusia (1971). There is considerable disagreement between the theoretical calculations of Copper (1962) for the 3p–4s transition in argon and those of other workers and his value has been

TABLE 7. THE OSCILLATOR STRENGTH MOMENTS S_r

atom	S_{-2}	S_{-1}	S_0	S_{+1}	S_{+2}
helium					
theor.	0.346	0.752	2	8.17	121
exp.	0.340	0.741	2.0	8.72	166
neon					
theor.	0.666	2.02	10	303	1.04×10^5
exp.	0.696	1.92	10.2	330	1.34×10^5
argon					
theor.	2.77	5.5	18	1.15×10^3	1.16×10^6
exp.	2.66	4.2	17.3	1.18×10^3	9.88×10^5
krypton					
theor.	4.18	7.86	36		
exp.	$\leqslant 3.5$	$\leqslant 5.5$	28.7 (sum of $n = 2, 3$ and 4 shells)		

For krypton, the higher experimental figures shown for the S_{-2} and S_{-1} moments are estimated upper limits.

TABLE 8. *f*-SUM FOR DISCRETE OUTER SHELL TRANSITIONS

atom	sum	transitions
helium	0.43 ± 0.03	1s–*n*p
neon	0.4 ± 0.1	2p–*n*s
		2p–*n*d
argon	0.7 ± 0.1	3p–*n*s
		3p–*n*d
krypton	0.6 ± 0.2	4p–*n*s
		4p–*n*d

discounted in estimating the *f*-sums. Data on the krypton resonance lines have been reported and reviewed by Griffin & Hutcheson (1969). Their best value data has been used here. Table 8 summarizes the contributions from the discrete transitions below the ionization thresholds used in the present *f*-sums. Hudson & Carter (1964) have measured the contribution from the continuum and autoionization lines for argon near 780 Å while Huffman *et al.* (1963*b*); Cook & Metzger (1964) and Carter & Hudson (1973) report and review similar studies for krypton. The calculations of Amusia (1971) suggest that for argon, $2p - ns$ ($n \geqslant 4$) will not contribute significantly to the *f*-summations. The equivalent transitions, 4s–*n*p and 2p–*n*s ($n \geqslant 5$) were also neglected in krypton.

As expected, the S_r values based on the experimental data are in good agreement with the Hartree–Fock calculations for helium. The discrepancies for S_{+1} and S_{+2} are accountable by the cross section discrepancies in the region of double ionization. For neon the S_0 sum of 10.2 can be separated into 8.6 associated with the $n = 2$ shell and 1.6 with the $n = 1$ shell; due allowance being made for the extrapolation of the $n = 2$ continuum beyond the $n = 1$ threshold. The theoretical values, after inclusion of the Pauli forbidden transitions in the partial summations appropriate from the individual shells, are 8.5 for the $n = 2$ shell and 1.5 for the $n = 1$ shell. For argon the agreement is not so good. After subtracting the Pauli forbidden transitions for the sum rules, the contributions remaining to the lines and continu awere found to be 8.30 ($n = 3$ shell) 8.28 ($n = 2$ shell) and 1.42 ($n = 1$ shell). Experimentally the contributions obtained are 8.51 ($n = 3$), 7.33 ($n = 2$) and 1.43 ($n = 1$) after making reasonable extrapolations beyond the ionization thresholds. Assuming that the major part of the unobserved oscillator strength required to bring the Σf to 18 comes from the $n = 2$ shell, there remains a suggestion that oscillator strength has been added to the $n = 3$ shell in excess of that required by the sum rules. This is in agreement with the prediction of Fano & Cooper (1968) that replacement of a one electron wavefunction model by a many electron treatment may be equivalent to a transfer of oscillator strength from inner to outer electrons. The $n = 1$ shell, being localized relatively close to the nucleus is not expected to be affected.

For krypton the analysis is incomplete in that we have only been able to include the $n = 4$, $n = 3$ and $n = 2$ shells in the summation. Taken together the outer two shells contribute 28.7, in good agreement with the value predicted by the Thomas–Reiche–Kuhn sum rule, after accounting for the contribution from Pauli forbidden transitions.

An examination of the variation of S_r from helium to krypton indicates that a marked reduction of S_{-2} and S_{-1} occurs away from the Hartree–Fock values. This would suggest that the atomic polarizabilities and the diamagnetic susceptibilities may be similarly reduced. In order to calculate the S_{+2} moments for helium, neon and argon an arbitrary cut-off energy of 100 keV was assumed in the summation from experimental data, beyond which scattering is expected to be dominant over photo-absorption. No attempt was made to calculate the S_{+2} and S_{+1} moments for krypton since there are no data for the high energy region (i.e. for $\epsilon \geqslant 10$ keV). The divergence of the summation at high energies suggests that the spectral density for large ϵ does not follow the non-relativistic predictions indicated by equation (14).

5. Conclusions and future work

The measurement of the total cross sections have been critically evaluated in order to provide a reliable set of data against which detailed calculation of atomic parameters can be tested. This has been carried out for helium down to the double ionization threshold at 79 eV. However, in compiling the data for the other inert

gases one has to rely on extrapolation from published cross section graphs and there is a need for published tabular data for detailed comparison of theory and experiment.

Attempts to separate out the total cross section data into specific subshells by extrapolation to the higher energy side of ionization thresholds indicates that further detailed study is required using photoelectron and photoion spectroscopy. The price to be paid for these experimental advances is a loss of signal against noise and the inability to evaluate partial cross section data. Again, reliable total cross section data are required to process the photoelectron spectra and experiments are now in progress in which the present absolute cross section data are exploited.

The electron synchrotron has made the continuous measurement of partial cross sections feasible and we have already reported data on the 3s cross section for argon (Houlgate, West, Codling & Marr 1974). A particularly interesting case where photoelectron spectroscopy can provide new information occurs at the onset of the 3d and 4d electron ionization of krypton and xenon respectively. The centrifugal barrier effect (Fano & Cooper 1968) causes the total cross section to be suppressed until well past threshold and the large peak seen in absorption has been attributed to the delayed $nd \rightarrow \epsilon f$ transitions. Photoelectron spectra taken with NINA indicate that direct ionization of the d electron only accounts for approximately three quarters of the total cross section. Because of 'polarization' of the 5s and 5p subshells in xenon by the 4d shell, these electrons are indirectly ionized and their contributions rise as the 4d threshold is passed. These results are the subject of a forthcoming publication (West, Woodruff, Codling & Houlgate 1976).

Angular distributions of photoelectrons from the 3p electron in argon (Houlgate *et al.* 1974) confirm the Cooper minimum in the total cross section at 200 Å as being due to the falling contribution in the $3p\text{–}\epsilon d$ channel. The behaviour of the asymmetry parameter β in the angular distribution curve as a function of photon energy is again better described by the r.p.a.e. calculations than by Hartree–Fock calculations. Recent theoretical studies on spin orbit interaction (Marr 1974; Walker & Weber 1974) predict that this can also cause large variations in β. Measurements to confirm these effects are being undertaken at the Daresbury synchroton.

This work has been supported by the Science Research Council as part of a continuing programme on the study of photo- and autoionization processes carried out by Reading University at the Synchrotron Radiation Facility. Technical support is gratefully acknowledged from the Daresbury Laboratory staff. The apparatus owed much to the skill of the J. J. Thomson Laboratory technicians, R. C. Chamberlain, B. Bennett and G. Folkerd.

PROCEEDINGS OF THE ROYAL SOCIETY A MATHEMATICAL, PHYSICAL & ENGINEERING SCIENCES

References

Altick, P. L. & Glassgold, A. E. 1964 *Phys. Rev.* **133**, A 632–646.

Amusia, M. Ya. 1971 Atomic Physics: II. *Proc. 2nd Int. Conf. on Atomic Physics* (ed. Woodgate & Sandars), pp. 249–269.

Amusia, M. Ya., Cherepkov, N. A. & Chernysheva, L. V. 1971 *Sov. Phys. J.E.T.P.* **33**, 90–6.

Amusia, M. Ya. 1974 *V.u.v. Physics, Proc. IVth Int. Conf. on v.u.v. Radiation Physics*, Hamburg, 22–26, July pp. 205–224. Braunschweig Pergamon Vieweg.

Anderson, D. K. 1965 *Phys. Rev.* **137** A, 21–6.

Axelrod, N. N. & Givens, M. P. 1959 *Phys. Rev.* **115**, 97.

Baker, D. J., Bedo, D. E. & Tomboulian, D. H. 1961 *Phys. Rev.* **124**, 1471–1476.

Balloffet, G., Romand, J. & Vodar, B. 1961 *C.r. hebd. Séanc. Acad. Sci., Paris* **252**, 413–441.

Bearden, A. J. 1966 *J. appl. Phys.* **37**, 1681–1692.

Bell, K. L. & Kingston, A. E. 1967 *Proc. Phys. Soc.* **90**, 901–7.

Bell, K. L. & Kingston, A. E. 1970 *J. Phys.* B 3, 1433–1436.

Bethe, H. A. & Salpeter, E. E. 1957 *Quantum mechanics of one- and two-electron atoms.* Springer-Verlag.

Blackwell, H. E., Bajwa, G. S., Shipp, G. S. & Weissler, G. L. 1964 *J. Quant. Spect. Rad. Trans.* **4**, 249–269.

Bohm, D. 1953 *Phys. Rev.* **92**, 626–636.

Bohm, D. & Pines, D. 1953 *Phys. Rev.* **92**, 609–626.

Burke, P. G. & Taylor, K. T. 1975 *J. Phys.* B **8**, 2620.

Cairns, R. B. & Samson, J. A. R. 1965 *J. geophys. Res.* **70**, 99–104.

Carlson, R. W., Judge, D. L., Ogawa, M. & Lee, L. C. 1973 *Appl. Opt.* **12**, 409–412.

Carter, V. L. & Hudson, R. D. 1973 *J. Opt. Soc. Am.* **63**, 733–735.

Chang, T. N. & Poe, R. T. 1975 *Phys. Rev.* A **11**, 191–199.

Codling, K. 1973 *Rep. Progr. Phys.* **36**, 541–624.

Comes, F. G. & Elzer, A. 1964 *Z. Natürforschung.* **199**, 721–727.

Compton, A. H. & Allison, S. K. 1967 *X-rays in theory and experiment*, Van Nostrand.

Connerade, J. P. & Mansfield, M. W. D. 1975 *Proc. R. Soc. Lond.* A **343**, 415–419.

Cook, G. R. & Metzger, P. H. 1964 *J. chem. Phys.* **41**, 321–326.

Cooper, J. W. 1962 *Phys. Rev.* **128**, 681–693.

Corney, A. 1970 *Advances in electronics and electron physics* **29**, 115–231. New York: Academic Press.

Crasemann, B. (ed.) 1975 *Atomic inner shell processes.* Vol. I. *Ionization transition probabilities.* New York: Academic Press.

Dershem, E. & Schein, M. 1931 *Phys. Rev.* **37**, 1238–1245.

Ditchburn, R. W. 1960 *Proc. Phys. Soc.* **75**, 461–462.

Ederer, D. L. & Tomboulian, D. H. 1964 *Phys. Rev.* **133** A, 1525–1532.

Fano, U. & Cooper, J. W. 1968 *Rev. mod. Phys.* **40**, 441–507.

Foster, E. W. 1964 *Rept Progr. Phys.* **27**, 469–551.

Froese-Fischer, C. 1972 *Atomic data*, vol. 4. New York: Academic Press.

Griffin, P. M. & Hutchesson, J. W. 1969 *J. Opt. Soc. Am.* **59**, 1607–1613.

Haensel, R., Keitel, G., Schreiber, P. & Kunz, C. 1969 *Phys. Rev.* **188**, 1375–1380.

Henke, B. L., Elgin, R. L., Lent, R. E. & Ledingham, R. B. 1967 *Norelco Reporter* **14**, 112–134.

Houlgate, R. G., West, J. B., Codling, K. & Marr, G. V. 1974 *J. Phys.* B **7**, L 470–473.

Huffman, R. E., Tanaka, Y. & Larrabee, J. C. 1963*a* *J. chem. Phys.* **32**, 902–909.

Huffman, R. E., Tanaka, Y. & Larrabee, J. C. 1963*b* *Proc. VIth Int. Conf. on Ionization Phenomena in Gases*, Paris, vol. 1, 145–148.

Hudson, R. D. & Carter, V. L. 1968 *J. Opt. Soc. Am.* **58**, 227–232.

Kuhn, H. G. & Vaughan, J. M. 1964 *Proc. R. Soc. Lond.* A **277**, 297–311.

Lang, J. & Watson, W. S. 1975 *J. Phys.* B **8**, L 339–343.

Lawrence, G. M. 1968 *Phys. Rev.* **175**, 40–44.

Lee, P. & Weissler, G. L. 1953 *Proc. R. Soc. Lond.* A **220**, 71–76.

Lee, P. & Weissler, G. L. 1955 *Phys. Rev.* **99**, 540–542.

PROCEEDINGS OF THE ROYAL SOCIETY A MATHEMATICAL, PHYSICAL & ENGINEERING SCIENCES

Lewis, E. L. 1967 *Proc. Phys. Soc.* **92**, 817–825.
Lowry, J. F., Tomboulian, D. H. & Ederer, D. L. 1961 *Phys. Rev.* **137**, A 1054–1057.
Lukirskii, A. P. & Zimkina, T. M. 1963 *Izv. Akad. Nauk. U.S.S.R.* **27**, 817–910.
Lukirskii, A. P., Brytov, I. A. & Zimkina, T. M. 1964 *Optics Spectrosc.* **17**, 234–237.
Marr, G. V. 1954 *Proc. R. Soc. Lond.* A **224**, 83–90.
Marr, G. V. 1967 *Photoionization processes in gases.* New York: Academic Press.
Marr, G. V. 1974 *J. Phys.* B **7**, L47–50.
Marr, G. V. & Creek, D. M. 1968 *Proc. R. Soc. Lond.* A **304**, 245–254.
Marr, G. V. & West, J. B. 1976 (to be published.)
Metzger, P. H. & Cook, G. R. 1965 *J. Opt. Soc. Am.* **55**, 516–520.
Miyake, K. P., Kato, R. & Yamashita, H. 1969 *Sci. Light* **18**, 39–56.
Ostrovskii, Yu. I. & Penkin, N. P. 1957 *Optika Spektrosk.* **3**, 193–201.
Pery-Thorne, A. & Garton, W. R. S. 1960 *Proc. Phys. Soc.* **76**, 833–843.
Piech, K. R. & Levinger, J. S. 1964 *Phys. Rev.* **135**, A 332–334.
Rau, M. R. P. & Fano, U. 1968 *Phys. Rev.* **167**, 7–10.
Rozhdestvenskii, D. 1912 *Ann. Physik, Leipzig* **39**, 307–345.
Rustgi, O. P. 1964 *J. Opt. Soc. Am.* **54**, 464–466.
Rustgi, O. P., Fisher, E. I. & Fuller, C. H. 1964 *J. Opt. Soc. Am.* **54**, 745–746.
Samson, J. A. R. 1966 *Advances in atomic and molecular physics*, vol. 2, pp. 177–261.
Samson, J. A. R. 1967 *Techniques of vacuum ultraviolet spectroscopy.* New York: Wiley.
Tanaka, Y., Huffmann, R. E. & Larrabee, J. C. 1962 *J. Quant. Spect. Rad. Trans.* **2**, 451–464.
Unsöld, A. 1955 *Physik der Sternatmosphoren.* Berlin: Springer Verlag.
Van Vleck, J. 1932 *Electric and magnetic susceptibilities.* Oxford: University Press.
Wainfan, N., Walker, W. C. & Weissler, G. L. 1955 *Phys. Rev.* **99**, 542–549.
Walker, T. E. H. & Waber, J. T. 1974 *J. Phys.* B **7**, 674–692.
Watson, W. S. 1972 *J. Phys.* B **5**, 2292–2303.
Weiss, A. W. 1967 *J. Res. natn. Bur. Stand.* **71** A, 163–168.
Weiss, A. W. 1970 *Nuclear Instrum. Methods* **90**, 121–131.
West, J. B., Codling, K. & Marr, G. V. 1974 *J. Phys.* E **1**, 137–144.
West, J. B., Woodruff, P. R., Codling, K. & Houlgate, R. G. 1976 *J. Phys.* B **9**, 407–410.
Wheaton, J. E. G. 1964 *Appl. Opt.* **3**, 1247–1249.
Wiese, W. L., Smith, M. W. & Glennan, B. M. 1966 *Atomic transition probabilities.* I. *H through Ne.* NRSRDS–NBS **4**.
Wiese, W. L., Smith, M. W. & Miles, B. M. 1969 *Atomic transition probabilities* II. *Na through Cu.* NSRDS–NBS **22**.
Wuilleumier, F. 1963 *C.r. hebd. Séanc. Acad. Sci., Paris* **257**, 855–858.
Wuilleumier, F. 1972 *Phys. Rev.* A **6**, 2067–2077.

PROCEEDINGS OF THE ROYAL SOCIETY A MATHEMATICAL, PHYSICAL & ENGINEERING SCIENCES